



Niobium nitride plasmonic perfect absorbers for tunable infrared superconducting nanowire photodetection

PHILIPP KARL,^{1,*}  SANDRA MENNLE,¹ MONIKA UBL,¹ PHILIPP FLAD,¹ JING-WEI YANG,^{2,3} TZU-YU PENG,^{2,3} YU-JUNG LU,^{2,3} AND HARALD GIESSEN¹ 

¹*4th Physics Institute and Research Center SCoPE, University of Stuttgart, Pfaffenwaldring 57, 70569 Stuttgart, Germany*

²*Research Center for Applied Sciences, Academia Sinica, Taipei 11529, Taiwan*

³*Department of Physics, National Taiwan University, Taipei 10617, Taiwan*

**philipp.karl@pi4.uni-stuttgart.de*

Abstract: Quantum technologies such as quantum computing and quantum cryptography exhibit rapid progress. This requires the provision of high-quality photodetectors and the ability to efficiently detect single photons. Hence, conventional avalanche photodiodes for single photon detection are not the first choice anymore. A better alternative are superconducting nanowire single photon detectors, which use the superconducting to normal conductance phase transition. One big challenge is to reduce the product between recovery time and detection efficiency. To address this problem, we enhance the absorption using resonant plasmonic perfect absorber effects, to reach near-100% absorption over small areas. This is aided by the high resonant absorption cross section and the angle insensitivity of plasmonic resonances. In this work we present a superconducting niobium nitride plasmonic perfect absorber structure and use its tunable plasmonic resonance to create a polarization dependent photodetector with near-100% absorption efficiency in the infrared spectral range. Further we fabricated a detector and investigated its response to an external light source. We also demonstrate the resonant plasmonic behavior which manifests itself through a polarization dependence detector response.

© 2021 Optical Society of America under the terms of the [OSA Open Access Publishing Agreement](#)

1. Introduction

Applications based on quantum technologies such as quantum computing [1,2] and quantum cryptography [3,4] require precise and high efficient photo detection. One way to achieve this utilizes so-called superconducting nanowire single photon detectors [5–7] (SNSPDs), which benefit from the superconducting to normal conductance phase transition. The big challenge is to reduce the product between the recovery time and detection efficiency [8]. Short wires will lead to faster recovery times, due to a small kinetic inductance. On the other hand, large photo-active areas with long wires will lead to a high detection efficient, but worsen the recovery time. One possible way to overcome this problem are plasmonic resonances, due to their high resonant absorption cross section. They represent an effective way to increase the efficiency of SNSPDs.

The ability of the detector to absorb the incident light and trigger a response is the absorption efficiency. This property depends on the material and the design of the detector. Therefore, SNSPDs are made from a large variety of superconducting materials such as molybdenum silicide [9], tungsten silicide [10], niobium titanium nitride [11–15], and niobium nitride (NbN) [16–18]. Many different types of SNSPDs have been created, such as waveguides [19], optical cavities [17,20], optical nanoantennas [21,22], and plasmonic nanostructures [5,6,23].

With the help of metallic nanostructures localized surface plasmons can be excited [24], which are already used in a variety applications [25–27]. Due to the high resonant absorption cross

section of plasmon resonances, one can achieve a high detection efficiency in combination with a small photo-active area to shorten recovery times.

In addition, the absorption of plasmonic nanostructures can be increased even further by using the so-called perfect absorber principle, leading to absorption up to almost 100% [28–30]. This effect also appears at high incident angles for TM polarization [31]. Perfect absorbers are already used for plasmonic applications, such as palladium perfect absorbers for gas sensing [32].

In this work we present a superconducting NbN photodetector and enhance its absorption by utilizing its plasmonic properties. With its tunable plasmonic resonance we create a polarization-dependent photodetector with near-100% absorption efficiency in the infrared spectral range.

2. Thin film production and nanofabrication

To obtain the optimum optical properties of our NbN nanostructures we need to be able to precisely define the structures. Therefore, we use electron beam lithography (EBL) in combination with plasma etching techniques, which allows us to take complete control of the fabrications process [33]. Figure 1 presents a schematic sketch of the used fabrication process.

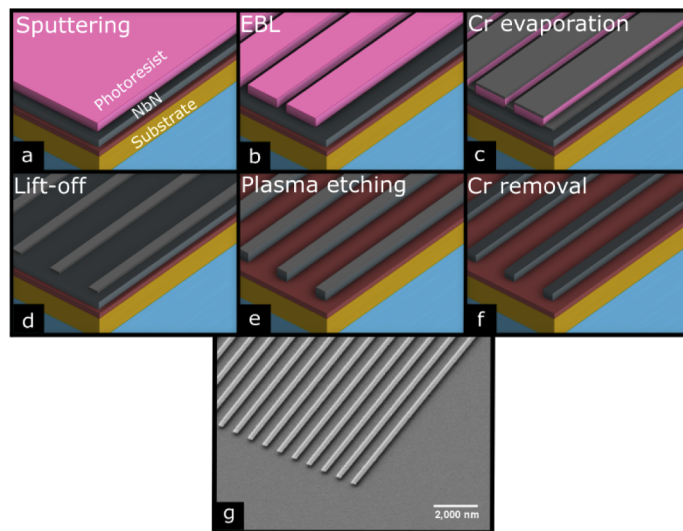


Fig. 1. Fabrication scheme of NbN nanostructures: (a) 20 nm thick NbN films are sputtered onto a perfect absorber substrate, subsequently a layer of high resolution photoresist is spin-coated on top. (b) Electron beam lithography exposure and development processes create an inverse pattern of the desired nanostructure. (c) A Cr layer is evaporated on top of the structure. (d) The Cr etching mask is created by removing the photoresist. (e) With plasma etching techniques, the nanoantennas are transferred to the NbN film. (f) Chemical Cr removal removes the etching mask. (g) Exemplary representation of the finished NbN nanostructures.

The perfect absorber substrate consists of a glass substrate with a 5 nm thick titanium (Ti) sticking layer, a 120 nm thick gold film and, a 100 nm thick aluminum oxide (Al_2O_3) dielectric spacer. The Ti and gold layer are evaporated via electron gun and the Al_2O_3 is deposited via atomic layer deposition (R-200 Advanced, Picosun), to obtain a clean and flat surface.

The NbN film was sputter-deposited onto the perfect absorber substrate. We use radio-frequency magnetron sputtering, with a NbN target, a deposition temperature of 800°C, a power of 120 W, a chamber pressure of $< 6 \times 10^{-8}$ torr, and with an argon/nitrogen flow rate of 24/1. We note that the properties of the NbN film can be varied with the target, growth temperature power,

and argon/nitrogen flow rate [34]. After the deposition, we vented the chamber with nitrogen at room temperature. These growth parameters ensure the highest possible critical temperature.

Before starting the EBL process a high resolution positive photoresist (AR-P 6200.04 (CSAR62), Allresist) and Espacer (Showa Denko) is spin-coated on top of the 20 nm thick NbN film, see Fig. 1(a). In Fig. 1(b) the photoresist is exposed via electron beam patterning (eLine Plus, Raith) and then developed to create an inverse image of the desired nanostructure in the photoresist. Figure 1(c) and (d) depict the evaporation and lift-off process of the Chromium (Cr) etching mask. First we use an electron gun to evaporate 50 nm Cr and subsequently n-ethyl-2-pyrrolidone based remover (Allresist) to remove undesired Cr in a lift-off process, leaving the finished Cr etching mask on the NbN film. The plasma etching creates the NbN nanostructure, see Fig. 1(e). In the end commercial Cr remover removes the etching mask, see Fig. 1(f). Figure 1(g) depicts an exemplary representation of the fabricated NbN nanostructures, using a scanning electron microscope (SEM) (S-4800, Hitachi). This process yields high-quality nanostructures, allows to adjust period and width of the nanowire arrays, and therefore enables us to tune the plasmonic resonance to desired wavelengths.

3. NbN perfect absorber plasmonics

In Fig. 2 we depict the absorption spectra of our 20 nm thick NbN nanowire arrays for different polarization angles, with different wire widths between 200 and 265 nm, a fixed periodicity of 500 nm, and normal incidence for the simulations as well as the measurements.

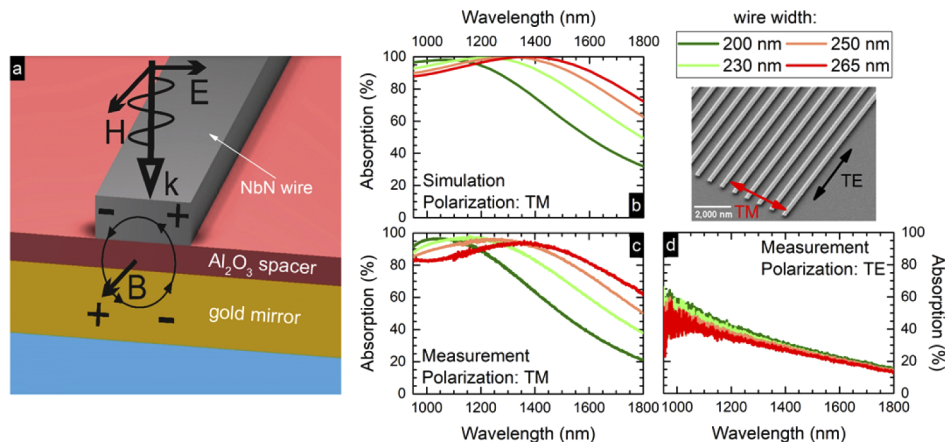


Fig. 2. Working principle and absorption spectra of the NbN plasmonic perfect absorber. (a) Schematic depiction of a NbN plasmonic perfect absorber. The plasmon oscillation leads to an antiphase oscillating mirror plasmon in the gold film, generating a circular current and hence a magnetic response. (b) Simulated absorption for a 20 nm thick NbN wire array on a perfect absorber substrate, with a fixed period of 500 nm and different wire widths, in TM polarization. The simulation reveals tunable and high absorbing plasmon resonances. (c) Measured absorption spectra of the simulated NbN structure in TM polarization. The spectra confirm the tunability of the plasmon resonance wavelength and near-100% absorption at resonance. (d) Measured spectra of the wire array in TE polarization, with lower absorption, due to the not excited plasmons.

To reach almost 100% absorbance at a certain wavelength we use the perfect absorber principle. Figure 2(a) depicts the schematic sketch of a perfect absorber. Phenomenologically, it can be imagined as follows. When perpendicular polarized light hits the NbN wire, localized surface plasmons are excited. The plasmon oscillation leads to an antiphase oscillating mirror plasmon in the gold film, generating a circular current and a magnetic response. As a simple mathematical

model the structure can be described as a medium with a magnetic permittivity $\mu(\lambda)$ and electric permittivity $\varepsilon(\lambda)$. By optimizing the geometric parameters (periodicity, wire width, and spacer thickness), both μ and ε can lead to impedance matching between the structure $Z_s = (\mu/\varepsilon)^{1/2}$ and the vacuum $Z_v = 1$. This impedance matching results in a suppressed reflection $R = (Z_v - Z_s)/(Z_v + Z_s)$. Moreover, the transmission in the infrared spectral range is blocked due to the thick gold mirror, which leads to an absorbance of $A = 1 - R - T = 1$ at the optimized wavelength [31].

To find these optimized parameters we carried out simulations using different geometries. For the simulations we use an in-house implementation of the Fourier modal method with a scattering matrix approach and 225 plane waves [35,36], where we utilize air as upper material and the perfect absorber as substrate. Figure 2(b) shows the simulated absorption spectra of four different nanowire arrays in TM polarization perpendicular to the wires, where the localized surface plasmons across the wires are excited. The simulations confirm tunable and over 99% absorbing plasmon resonances, which are fundamental dipole resonances [37], between wavelengths of 1000 and 1400 nm.

In Fig. 2(c) we plot a Fourier-transform infrared spectroscopy spectrometer (FTIR) measurement (Bruker Vertex 80 microscope Hyperion 3000) of the nanostructures, which exhibit an absorption of over 95%, in which a blank piece of the perfect absorber substrate on the same sample is used as a reference. This highly absorbing plasmon resonance can further be tuned to lower and higher frequencies by changing for example the wire width, to reach important telecommunication wavelengths with absorption efficiencies of over 95%. Due to the excited mirror plasmon in the gold of the perfect absorber structure, the strong absorption enhancement for TM polarization also applies to moderately tilted angles [31,38]. The small mismatches between the simulation and the real samples can be explained by a slightly imperfect geometry.

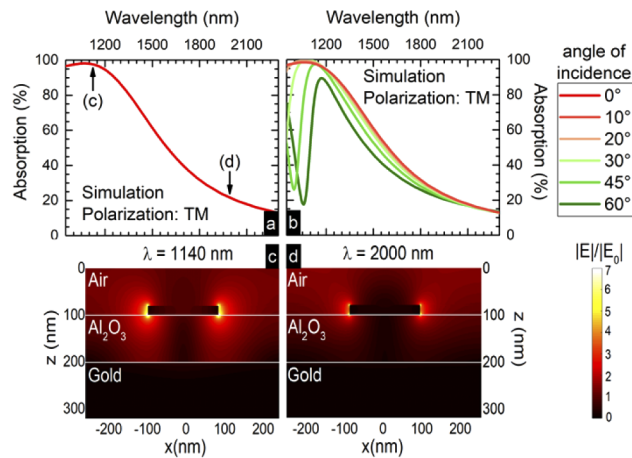


Fig. 3. Electric field enhancement for the NbN nanostructures and angle dependence. (a) Simulated absorption spectrum for a 20 nm thick NbN wire array on a perfect absorber substrate, with a fixed period of 500 nm and a wire width of 200 nm in TM polarization and normal incidence. (b) Simulated absorption spectra for different angles of incidence. The absorption spectra hardly change for angles of up to 20° and retains its high absorption even for large angles, due to the perfect absorber substrate and the high losses of the material. (c) and (d) electric field enhancement distributions for the simulated NbN wire array once for 1140 nm (at resonance) and once for 2000 nm (off resonance), for normal incidence. They confirm that the absorption of the incoming light happens almost completely in the NbN wire on top of the perfect absorber substrate and therefore there are no parasitic absorption in the dielectric spacer or gold mirror below.

Figure 2(d) demonstrates the FTIR measurement in TE polarization. The absorbance in this polarization is smaller, due to the absence of excited plasmons and is caused by the high losses in material [39]. This difference proves that the high absorption is of plasmonic nature.

Figure 3 depicts the angle of incidence dependence and the electric field for the NbN nanostructures. In Fig. 3(a) we plot the simulated absorption spectrum for a 20 nm thick NbN wire array on a perfect absorber substrate, with a fixed period of 500 nm and a wire width of 200 nm in TM polarization and normal incidence, which corresponds to the fabricated detector. For normal incidence we reach over 99% absorbance at the plasmon resonance. In Fig. 3(b) we present the simulated absorption spectra for different angles of incidence. The absorption spectra hardly change for angles of up to 20° and retain their high absorption values even for large angles, due to the perfect absorber substrate [31,38] and the high losses of the material. This excellent angle independence up to large values aid in using our detector concept in combination with high NA objectives, which can focus light to a diffraction limited spot. This will enable in the future extremely small (μm^2) detector areas with ultra-low kinetic inductance and capacitance, which will increase the detector speed and shortens its recovery time.

Figure 3(c) shows the electric field enhancement for the NbN nanostructure at 1140 nm. We confirm a strong interaction between the incoming light and the NbN wire. The absorption of the incoming light happens almost completely in the NbN (where the near field exhibits hot spots) on top of the perfect absorber substrate and therefore there are nearly no parasitic absorptions in the dielectric spacer or in the gold mirror below. The interaction at 2000 nm is weaker compared to 1140 nm, due to the smaller absorption, compare Fig. 3(d).

4. Detector design and characterization

4.1. Design, absorption and superconducting properties

For the superconducting perfect absorber photodetector, a 20 nm thick NbN film on top of a perfect absorber substrate is used. The detector itself has a wire width of 200 nm and a periodicity of 500 nm, with an active area of $30 \times 30 \mu\text{m}^2$, see Fig. 4(c). It is a grid with connections between the different wires to form a continuous meander and uses four large gold contact pads to perform four-point resistivity measurements, see Fig. 5.

Figure 4 depicts the absorption spectra and meander design of the active area. In Fig. 4(a) we demonstrate the high absorption spectrum for our fabricated detector structure for TM and TE polarization. For TM polarization we excite the localized plasmons across the NbN wires and reach an absorption of up to 95%. For TE polarization the absorption is expectedly lower and caused by the high losses in the material [39]. A polarization independent design could use disks, square patches, crosses, or checkerboard-like perpendicular lattices [38]. Figure 4(b) compares the measured spectra with the simulated ones and shows a good agreement for both polarizations. The measured active area can be seen in Fig. 4(c).

In Fig. 5 we demonstrate the superconducting properties and design of the NbN detector. Figure 5(a) shows the normalized resistance of the detector structure measured in a four-point resistivity measurement. The broad superconducting transition is clearly visible around 11 K. This critical temperature is a good result and in the expected range, which is slightly below the bulk value ($T_c = 16.5$ K), due to the fact that the critical temperature of thin films is in generally lower than its literature bulk value [40,41]. Figure 5(b) depicts the normalized magnetic moment obtained via a superconducting quantum interference device measurement, which also exhibit a superconducting behavior below 11 K. In Fig. 5(c) the critical current of the measured detector is displayed, which confirms the critical temperature of 11 K. The entire manufactured detector structure can be seen in Fig. 5(d).

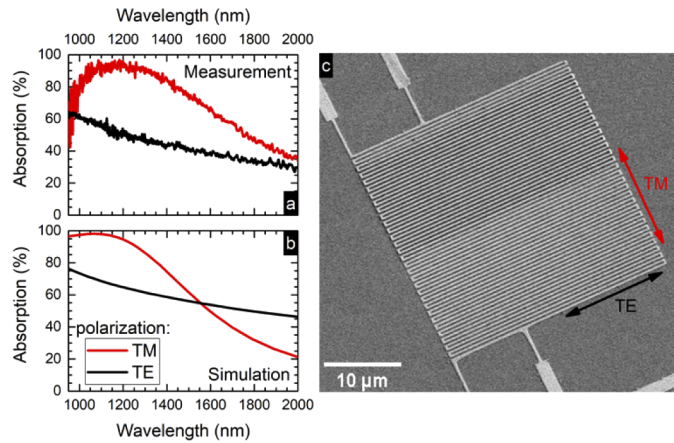


Fig. 4. Absorption spectra and design of the 20 nm thick NbN detector, with a period of 500 nm, wire thickness of 200 nm and an active area of $30 \times 30 \mu\text{m}^2$. (a) Measured absorption spectra of the detector, which confirm the enhancement of the absorption by utilization the plasmonic properties of NbN and perfect absorber principle, which leads to near-100% absorption in the optimized frequency range. (b) Simulated absorption spectrum of the detector, which reveal a good agreement between simulated and measured data. (c) SEM image of the active area of the NbN detector.

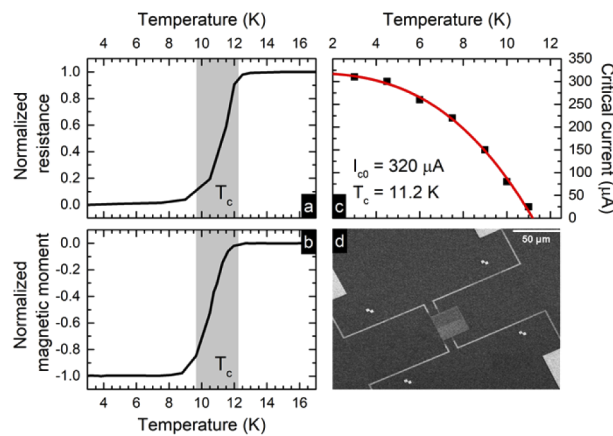


Fig. 5. Superconducting properties and design of the 20 nm thick NbN detector. (a) Normalized resistance of the structure measured by performing four-point resistivity measurement. The broad superconducting transition is clearly visible around 11 K. (b) SQUID measurement of the 20 nm thick NbN film. The depicted normalized magnetic moment also shows a superconducting behavior below 11 K. (c) Critical current of the measured detector, which confirms the critical temperature of 11 K. (d) SEM image of the entire detector structure. The active area is connected with four large gold pad contacts in order to be able to carry out the four-point resistivity measurement.

4.2. Detector response

To demonstrate the detector response to an external light source and the plasmonic role in its absorption behavior we use a cryostat with optical access, as well as a KEITHLEY 2611B current source and a KEITHLEY 2182A nanovoltmeter to measure the change in its resistance.

When the NbN nanowire is hit by a photon, a hot spot is created due to the disturbance and heating of cooper pairs. The supercurrent will be forced to flow around this region as it is more resistive, which will increase the current density of the surrounding area. If the bias current exceeds the superconducting critical current, the wire will switch to its normal conductive state, which will result in a voltage drop.

Figure 6 confirms the efficiency and functionality of the superconducting NbN detector structure with a laser source (Toptica ECDL Pro) and wavelength of $\lambda = 1140$ nm for various laser powers, in the superconducting state at 3.5 K, 8.5 K, and the normal conducting state at 20 K. To reach the strongest possible response we measured the detector response represented by a voltage drop at a fixed laser power of 22.5 μ W at 3.5 K in TM polarization for different applied currents. The maximum response of the system arises slightly below the critical current at 220 μ A. If the current is too small, the detector does not switch to the normal conducting state and if the current is too strong, some parts are already normally conducting, leading to weaker responses, see Fig. 6(a).

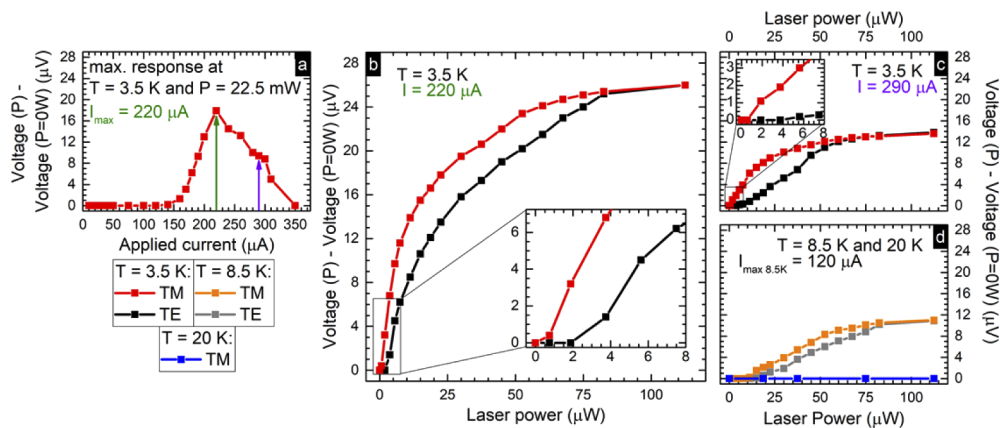


Fig. 6. Detector response. (a) Measured detector response represented by a voltage drop for different applied currents at 1140 nm, 3.5 K and a constant laser power of 22.5 μ W. The maximum response of the system arises slightly below the critical current at 220 μ A. If the current is too low, the detector does not switch to the normal conducting state and if the current is too strong, some parts are already normal conducting. (b) The detector response at 3.5 K and an applied current of 220 μ A over a wide laser power range for both polarization angles. For higher powers, the response is indistinguishable due the system is completely in its normal conducting state. The results indicate the polarization dependence of the detector response and proves the plasmonic behavior. (c) Measured detector response for an applied current of 290 μ A, at 3.5 K for different the laser powers. This confirm the result from (a), and the overall stronger response with 220 μ A also enables smaller laser powers to be detected, see insets. (d) Voltage drop for 8.5 K, with optimized applied current and 20 K. The response of the detector is smaller compared to 3.5 K, probably due to the fact that small parts of the structure are no longer superconducting. The detector shows no response its normal conducting state at 20 K.

In Fig. 6(b) we demonstrate the detector response at 3.5 K with an applied current of 220 μ A while illuminating the photodetector with the laser source for various laser powers. The difference in the absorption efficiency can be directly observed by a measured voltage drop. This

confirms that our system can distinguish between the polarizations of the incoming light, due to the stronger response for the TM polarization, caused by the higher absorption. For higher powers, the response is indistinguishable due the system is completely in its normal conducting state.

Figure 6(c) confirms the results from Fig. 6(a) and plots the detector response 3.5 K with an applied current of 290 μA . The result is basically the same as for 220 μA , but the voltage drop is smaller. The overall stronger response using 220 μA also enables smaller laser powers to be detected, see insets.

The detector performance for higher temperatures is depicted in Fig. 6(d). The response of the detector at 8.5 K is smaller compared to 3.5 K, due to the fact that small parts of the structure are no longer superconducting and the detector shows no response in its normal conducting state at 20 K.

5. Conclusion

In summary, we fabricated a superconductivity niobium nitride detector for infrared photodetection by utilizing a plasmonic perfect absorber geometry to reach almost 100% absorption. In addition, our structure is not only able to detect the incoming light, it also able to differentiate its polarization, due to the stronger absorption and response for the TM polarization. The perfect absorber geometry allows also for a nearly angle independent absorbance, which will aid smaller and faster detectors in combination with high NA optics in the future [42,43].

Funding. Academia Sinica (AS-CDA-108-M08); Ministry of Science and Technology, Taiwan (MOST-109-2112-M-001-043-MY3); Open Access Fund University of Stuttgart; Ministerium für Wissenschaft, Forschung und Kunst Baden-Württemberg (IQST); Baden-Württemberg Stiftung; Carl-Zeiss-Stiftung; Deutsche Forschungsgemeinschaft; European Research Council (Complexplas).

Acknowledgments. We thank O. Iakutkina from the 1st Physics Institute (University of Stuttgart) for help with the resistivity measurements and T. Weiss from the 4th Physics Institute (University of Stuttgart) for help with the S-Matrix simulations.

Disclosures. The authors declare no conflicts of interest.

Data availability. Data underlying the results presented in this paper are not publicly available at this time but may be obtained from the authors upon reasonable request.

References

1. E. Knill, R. Laflamme, and G. J. Milburn, "A scheme for efficient quantum computation with linear optics," *Nature* **409**(6816), 46–52 (2001).
2. J. L. O'Brien, "Optical Quantum Computing," *Science* **318**(5856), 1567–1570 (2007).
3. K. Takemoto, Y. Nambu, T. Miyazawa, Y. Sakuma, T. Yamamoto, S. Yoroza, and Y. Arakawa, "Quantum key distribution over 120 km using ultrahigh purity single-photon source and superconducting single-photon detectors," *Sci. Rep.* **5**(1), 14383 (2015).
4. H. K. Lo, M. Curty, and K. Tamaki, "Secure quantum key distribution," *Nat. Photonics* **8**(8), 595–604 (2014).
5. A. Eftekharian, H. Atikian, and A. H. Majedi, "Plasmonic superconducting nanowire single photon detector," *Opt. Express* **21**(3), 3043–3054 (2013).
6. C. M. Natarajan, M. G. Tanner, and R. H. Hadfield, "Superconducting nanowire single-photon detectors: physics and applications," *Supercond. Sci. Technol.* **25**(6), 063001 (2012).
7. G. N. Gol'tsman, O. Okunev, G. Chulkova, A. Lipatov, A. Semenov, K. Smirnov, B. Voronov, A. Dzardanov, C. Williams, and R. Sobolewski, "Picosecond superconducting single-photon optical detector," *Appl. Phys. Lett.* **79**(6), 705–707 (2001).
8. A. J. Kerman, E. A. Dauler, J. K. W. Yang, K. M. Rosfjord, V. Anant, K. K. Berggren, G. N. Gol'tsman, and B. M. Voronov, "Constriction-limited detection efficiency of superconducting nanowire single-photon detectors," *Appl. Phys. Lett.* **90**(10), 101110 (2007).
9. V. B. Verma, B. Korzh, F. Bussières, R. D. Horansky, S. D. Dyer, A. E. Lita, I. Vayshenker, F. Marsili, M. D. Shaw, H. Zbinden, R. P. Mirin, and S. W. Nam, "High-efficiency superconducting nanowire single-photon detectors fabricated from MoSi thin-films," *Opt. Express* **23**(26), 33792–33801 (2015).
10. F. Marsili, V. B. Verma, J. A. Stern, S. Harrington, A. E. Lita, T. Gerrits, I. Vayshenker, B. Baek, M. D. Shaw, R. P. Mirin, and S. W. Nam, "Detecting single infrared photons with 93% system efficiency," *Nat. Photonics* **7**(3), 210–214 (2013).

11. I. E. Zadeh, J. W. N. Los, R. B. M. Gourgues, V. Steinmetz, G. Bulgarini, S. M. Dobrovolskiy, V. Zwiller, and S. N. Dorenbos, "Single-photon detectors combining high efficiency, high detection rates, and ultra-high timing resolution," *APL Photonics* **2**(11), 111301 (2017).
12. S. Miki, T. Yamashita, H. Terai, and Z. Wang, "High performance fiber-coupled NbTiN superconducting nanowire single photon detectors with Gifford-McMahon cryocooler," *Opt. Express* **21**(8), 10208–10214 (2013).
13. N. R. Gemmill, M. Hills, T. Bradshaw, T. Rawlings, B. Green, R. M. Heath, K. Tsimvraikidis, S. Dobrovolskiy, V. Zwiller, S. N. Dorenbos, M. Crook, and R. H. Hadfield, "A miniaturized 4 K platform for superconducting infrared photon counting detectors," *Supercond. Sci. Technol.* **30**(11), 11LT01 (2017).
14. S. Steinhauer, L. Yang, S. Gyger, T. Lettner, C. Errando-Herranz, K. D. Jöns, M. A. Baghban, K. Gallo, J. Zichi, and V. Zwiller, "NbTiN thin films for superconducting photon detectors on photonic and two-dimensional materials," *Appl. Phys. Lett.* **116**(17), 171101 (2020).
15. S. Gyger, J. Zichi, L. Schweickert, A. W. Elshaari, S. Steinhauer, S. F. Covre da Silva, A. Rastelli, V. Zwiller, K. D. Jöns, and C. Errando-Herranz, "Reconfigurable quantum photonics with on-chip detectors," arXiv 1–31 (2020).
16. D. Rosenberg, A. J. Kerman, R. J. Molnar, and E. A. Dauler, "High-speed and high-efficiency superconducting nanowire single photon detector array," *Opt. Express* **21**(2), 1440–1447 (2013).
17. W. Zhang, L. You, H. Li, J. Huang, C. Lv, L. Zhang, X. Liu, J. Wu, Z. Wang, and X. Xie, "NbN superconducting nanowire single photon detector with efficiency over 90% at 1550 nm wavelength operational at compact cryocooler temperature," *Sci. China Phys. Mech. Astron.* **60**(12), 120314 (2017).
18. A. Mukhtarova, L. Redaelli, D. Hazra, H. Machhadani, S. Lequien, M. Hofheinz, J.-L. Thomassin, F. Gustavo, J. Zichi, V. Zwiller, E. Monroy, and J.-M. Gérard, "Polarization-insensitive fiber-coupled superconducting-nanowire single photon detector using a high-index dielectric capping layer," *Opt. Express* **26**(13), 17697–17704 (2018).
19. J. P. Sprengers, A. Gaggero, D. Sahin, S. Jahanmirinejad, G. Frucci, F. Mattioli, R. Leoni, J. Beetz, M. Lermer, M. Kamp, S. Höfling, R. Sanjines, and A. Fiore, "Waveguide superconducting single-photon detectors for integrated quantum photonic circuits," *Appl. Phys. Lett.* **99**(18), 181110 (2011).
20. K. M. Rosfjord, J. K. W. Yang, E. A. Dauler, A. J. Kerman, V. Anant, B. M. Voronov, G. N. Gol'tsman, and K. K. Berggren, "Nanowire single-photon detector with an integrated optical cavity and anti-reflection coating," *Opt. Express* **14**(2), 527–534 (2006).
21. X. Hu, E. A. Dauler, R. J. Molnar, and K. K. Berggren, "Superconducting nanowire single-photon detectors integrated with optical nano-antennae," *Opt. Express* **19**(1), 17–31 (2011).
22. R. M. Heath, M. G. Tanner, T. D. Drysdale, S. Miki, V. Giannini, S. A. Maier, and R. H. Hadfield, "Nanoantenna enhancement for telecom-wavelength superconducting single photon detectors," *Nano Lett.* **15**(2), 819–822 (2015).
23. A. Farag, M. Ubl, A. Konzelmann, M. Hentschel, and H. Giessen, "Utilizing niobium plasmonic perfect absorbers for tunable near- and mid-IR photodetection," *Opt. Express* **27**(18), 25012–25021 (2019).
24. L. Novotny and B. Hecht, *Principles of Nano-Optics* (Cambridge University, 2006), (May).
25. F. Sterl, N. Strohfeldt, S. Both, E. Herkert, T. Weiss, and H. Giessen, "Design Principles for Sensitivity Optimization in Plasmonic Hydrogen Sensors," *ACS Sens.* **5**(4), 917–927 (2020).
26. M. Sturaro, E. D. Gaspera, N. Michieli, C. Cantalini, S. M. Emamjomeh, M. Guglielmi, and A. Martucci, "Degenerately Doped Metal Oxide Nanocrystals as Plasmonic and Chemoresistive Gas Sensors," *ACS Appl. Mater. Interfaces* **8**(44), 30440–30448 (2016).
27. X. Yin, T. Steinle, L. Huang, T. Taubner, M. Wuttig, T. Zentgraf, and H. Giessen, "Beam switching and bifocal zoom lensing using active plasmonic metasurfaces," *Light: Sci. Appl.* **6**(7), e17016 (2017).
28. K. Chen, R. Adato, and H. Altug, "Dual-band perfect absorber for multispectral plasmon-enhanced infrared spectroscopy," *ACS Nano* **6**(9), 7998–8006 (2012).
29. N. I. Landy, S. Sajuyigbe, J. J. Mock, D. R. Smith, and W. J. Padilla, "Perfect Metamaterial Absorber," *Phys. Rev. Lett.* **100**(20), 207402 (2008).
30. A. Tittl, A. K. U. Michel, M. Schäferling, X. Yin, B. Gholipour, L. Cui, M. Wuttig, T. Taubner, F. Neubrech, and H. Giessen, "A Switchable Mid-Infrared Plasmonic Perfect Absorber with Multispectral Thermal Imaging Capability," *Adv. Mater.* **27**(31), 4597–4603 (2015).
31. N. Liu, M. Mesch, T. Weiss, M. Hentschel, and H. Giessen, "Infrared perfect absorber and its application as plasmonic sensor," *Nano Lett.* **10**(7), 2342–2348 (2010).
32. A. Tittl, P. Mai, R. Taubert, D. Dregely, N. Liu, and H. Giessen, "Palladium-based plasmonic perfect absorber in the visible wavelength range and its application to hydrogen sensing," *Nano Lett.* **11**(10), 4366–4369 (2011).
33. S. Bagheri, C. M. Zgrabik, T. Gissibl, A. Tittl, F. Sterl, R. Walter, S. De Zuani, A. Berrier, T. Stauden, G. Richter, E. L. Hu, and H. Giessen, "Large-area fabrication of TiN nanoantenna arrays for refractory plasmonics in the mid-infrared by femtosecond direct laser writing and interference lithography [Invited]," *Opt. Mater. Express* **5**(11), 2625–2633 (2015).
34. Y. J. Lu, R. Sokhoyan, W. H. Cheng, G. K. Shirmanesh, A. R. Davoyan, R. A. Pala, K. Thyagarajan, and H. A. Atwater, "Dynamically controlled Purcell enhancement of visible spontaneous emission in a gated plasmonic heterostructure," *Nat. Commun.* **8**(1), 1631 (2017).
35. T. Weiss, N. A. Gippius, S. G. Tikhodeev, G. Granet, and H. Giessen, "Efficient calculation of the optical properties of stacked metamaterials with a Fourier modal method," *J. Opt. A: Pure Appl. Opt.* **11**(11), 114019 (2009).
36. T. Weiss, G. Granet, N. A. Gippius, S. G. Tikhodeev, and H. Giessen, "Matched coordinates and adaptive spatial resolution in the Fourier modal method," *Opt. Express* **17**(10), 8051–8061 (2009).

37. L. Novotny, "Effective Wavelength Scaling for Optical Antennas," *Phys. Rev. Lett.* **98**(26), 266802 (2007).
38. R. Walter, A. Tittl, A. Berrier, F. Sterl, T. Weiss, and H. Giessen, "Large-area low-cost tunable plasmonic perfect absorber in the near infrared by colloidal etching lithography," *Adv. Opt. Mater.* **3**(3), 398–403 (2015).
39. P. Karl, M. Ubl, M. Hentschel, P. Flad, Z. Y. Chiao, J. W. Yang, Y. J. Lu, and H. Giessen, "Optical properties of niobium nitride plasmonic nanoantennas for the near- and mid-infrared spectral range," *Opt. Mater. Express* **10**(10), 2597–2606 (2020).
40. S. J. Lee and J. B. Ketterson, "Critical sheet resistance for the suppression of superconductivity in thin Mo-C films," *Phys. Rev. Lett.* **64**(25), 3078–3081 (1990).
41. T. Shiino, S. Shiba, N. Sakai, T. Yamakura, L. Jiang, Y. Uzawa, H. Maezawa, and S. Yamamoto, "Improvement of the critical temperature of superconducting NbTiN and NbN thin films using the AlN buffer layer," *Supercond. Sci. Technol.* **23**(4), 045004 (2010).
42. L. Bremer, K. Weber, S. Fischbach, S. Thiele, M. Schmidt, A. Kaganskiy, S. Rodt, A. Herkommer, M. Sartison, S. L. Portalupi, P. Michler, H. Giessen, and S. Reitzenstein, "Quantum dot single-photon emission coupled into single-mode fibers with 3D printed micro-objectives," *APL Photonics* **5**(10), 106101 (2020).
43. M. Sartison, K. Weber, S. Thiele, L. Bremer, S. Fischbach, T. Herzog, S. Kolatschek, M. Jetter, S. Reitzenstein, A. Herkommer, P. Michler, S. Luca Portalupi, and H. Giessen, "3D printed micro-optics for quantum technology: Optimised coupling of single quantum dot emission into a single-mode fibre," *Light Adv. Manuf.* **2**(1), 1–17 (2021).